Profiling of objects with height steps by wavelet analysis of shadow moiré fringes

Quan, Chenggen; Fu, Yu; Tay, Cho Jui; Tan, Jia Min

2005

Quan, C., Fu, Y., Tay, C. J., & Tan, J. M. (2005). Profiling of objects with height steps by wavelet analysis of shadow moiré fringes. Applied Optics, 44(16), 3284-3290.

https://hdl.handle.net/10356/91921

https://doi.org/10.1364/AO.44.003284

Profiling of objects with height steps by wavelet analysis of shadow moiré fringes

Chenggen Quan, Yu Fu, Cho Jui Tay, and Jia Min Tan

A temporal wavelet analysis algorithm is proposed for shadow-moiré-based three-dimensional surface profiling on objects having discontinuous height steps. A grating is positioned close to an object, and its shadow is observed through the grating. The moiré fringe patterns vary when the grating is in-plane rotating. A series of fringe patterns are captured by a CCD camera at different rotating angles. Phase values are evaluated point by point with the continuous wavelet transform. From the phase values of each point on the object, the distance between the object and the grating can be retrieved. The surface profile is obtained without temporal or spatial phase unwrapping. This technique is applicable to objects with discontinuous height steps, which are impossible to measure with conventional shadow moiré topography. Two specimens are tested to demonstrate the validity of the method: One is an object with a height step of 1.6 mm, and another is a small coin with unevenness of less than 0.2 mm. The experimental results are compared with test results by use of the mechanical stylus method.

OCIS codes: 120.4120, 100.7410, 120.6650, 100.5070.

1. Introduction

Moiré topography is a noncontact method for three-dimensional (3-D) profile measurement proposed by Meadows *et al.*[1] and Takasaki[2] in the early 1970s. Depending on the optical arrangement, it can be classified as projection moiré or shadow moiré. Shadow moiré topography is a relatively cheap and simple technique requiring only an ordinary white-light source, a periodic transmission grating, and a camera (see Fig. 1). In this setup a periodic grating is placed closely in front of the test object. With light illuminating the test object at an oblique angle through the grating, the shadow of the grating is cast onto the object surface. The shadow lines are distorted in accordance with the profile of the test surface. Moiré fringes, which are loci of the surface depth with respect to the grating plane, are observed at the image plane of the camera owing to light interference between the grating and the shadow lines. One shortcoming of shadow moiré is the difficulty of determining whether the surface is convex or concave from one fringe pattern. Compared with other optical techniques, shadow moiré is also less sensitive. To achieve high-resolution measurements, researchers applied different types of the phase-shifting technique[3–8] to moiré topography in the 1990s. One can calculate a wrapped phase map that encodes the profile information by acquiring several images with the fringe shifted by known phase steps. However, if the object contains height steps or surface discontinuities, correct spatial phase unwrapping may become impossible[9] when the sensitivity factor of the shadow moiré technique is not coarse enough. Moreover, with the shadow moiré technique, phase shifting is not easily accomplished.[3]

One of the solutions is to select the grating and geometric parameters properly so that the phase change due to the height steps is less than 2π; however, it will reduce the sensitivity of measurement and the phase-unwrapping process will still have problems when two separated surfaces are measured simultaneously. To solve this problem, Jin *et al.*[10] developed a novel approach, called the frequency-sweeping method, to extract the phase in the temporal domain. The frequency of the grating is varied by rotation of the grating, and a series of fringe patterns is captured during the rotation. The phase value on each pixel, which contains height information, is calculated from intensity variation.[11,12] The concept is similar to wavelength-shift speckle interferome-

The authors are with the Department of Mechanical Engineering, National University of Singapore, 10 Kent Ridge Crescent, Singapore 119260. The e-mail address of C. Quan is mpeqcg@nus.edu.sg.

Received 15 June 2004; revised manuscript received 14 December 2004; accepted 5 January 2005.

0003-6935/05/163284-07$15.00/0

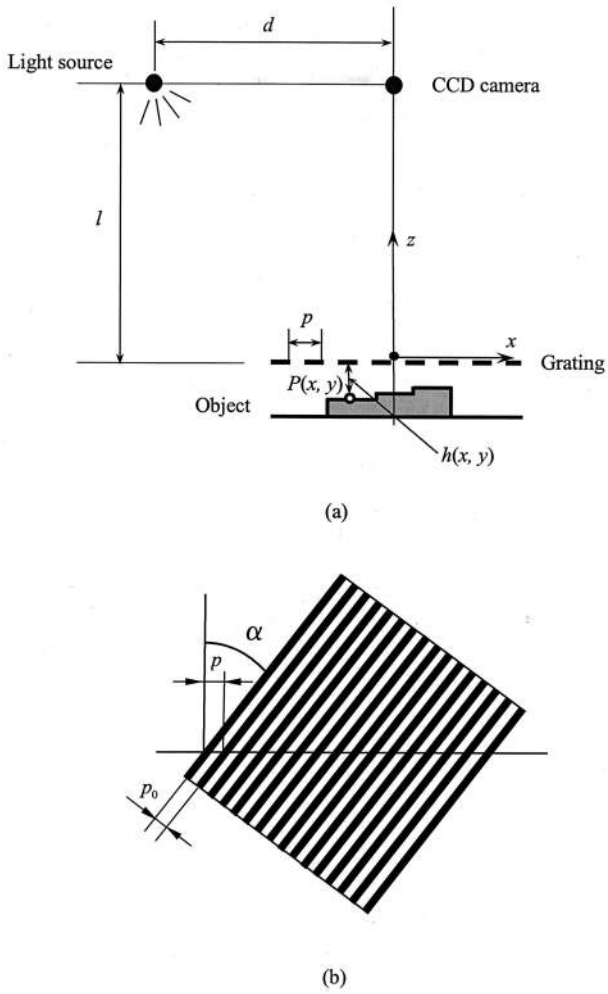

Fig. 1. Schematic layout of the shadow moiré system.

try,[13,14] which varies the wavelength of a laser for profile measurement. Although some temporal phase analysis algorithms[15] have been introduced, the Fourier transform[16] is still the predominant method in temporal phase analysis. The intensity fluctuation of each pixel is first transformed, and one side of the spectrum is filtered with a bandpass filter. The filtered spectrum is inverse transformed to obtain a wrapped phase. The phase values are then unwrapped along the time axis at each pixel independently of other pixels in the image. However, in the frequency-sweeping approach, the frequency variation of the grating is not linear during rotation. To obtain a single frequency of intensity variation, researchers adopted nonconsistent angle steps for linearization. However, this increases the difficulty of automatic measurement as the rotating speed of the grating and the capturing rate of the CCD camera are normally consistent. This shortcoming of the frequency-sweeping method can be overcome by the use of temporal wavelet analysis.

Wavelet transform[17] is a new and robust mathematic tool for signal analysis. Continuous wavelet transform (CWT) was also used for phase extraction on different types of the open-fringe interferogram or fringe pattern with spatial carriers.[18–21] These applications use one-dimensional CWT along a spatial axis. One can retrieve the phase by extracting the ridge of wavelet coefficients. However, all these techniques extract the phase in the spatial domain. Colonna de Lega and others[22–24] applied the temporal wavelet transform to speckle interferometry, and some preliminary results were presented. In the present study a series of moiré fringe patterns are captured at different angles of the grating. The CWT is applied to the intensity variation of each pixel. The instantaneous frequency of intensity variation is obtained by extraction of the ridge of the wavelet coefficients, followed by an integration process to retrieve the phase change between different angles. The distance between the object and the grating is then iterated by the least-squares method.

2. Theoretical Analysis

The schematic layout of the shadow moiré setup for contour measurement is shown in Fig. 1(a). A grating is placed in the xy plane and close to the object surface. A camera and a light source are placed at distance l from the grating with a pitch p. The intensity distribution captured by a CCD camera is governed by the following equation[10]:

$$I(x, y) = A(x, y) + B(x, y)\cos \phi_{xy} = A(x, y) + B(x, y)\cos\left\{\frac{2\pi h(x, y)d}{p[l + h(x, y)]}\right\}, \quad (1)$$

where $A(x, y)$ and $B(x, y)$ are the intensity bias and modulation factor, respectively. $h(x, y)$ is the distance from the grating plane to a point $P(x, y)$ on the object, and d is the distance between the light source and the camera. When the grating is rotated at certain angle α [see Fig. 1(b)], Eq. (1) can be rearranged as

$$I(x, y) = A(x, y) + B(x, y)\cos\left[\frac{2\pi \cos \alpha}{p_0} H(x, y)\right], \quad (2)$$

where P_0 is the physical pitch of the grating, and $H(x, y) = h(x, y)d/[l + h(x, y)]$ is a parameter related to the profile. A series of fringe patterns are recorded during rotation, and, at each pixel, the history of intensity variation is analyzed with the CWT.

A wavelet $\Psi(t)$ is a function with a zero average and centered in the neighborhood of $t = 0$. A set of wavelet function $\Psi_{a,b}(t)$ can be constructed with elementary operations consisting of time shifts and scaling (i.e., dilation or contraction). The set of wavelets is defined by

$$\psi_{a,b}(t) = \frac{1}{\sqrt{a}}\psi\left(\frac{t - b}{a}\right), \qquad b \in R,\ a > 0, \quad (3)$$

where a is the scaling factor and b is the time shift.

The CWT decomposes a signal over dilated and translated wavelets $\Psi_{a,b}(t)$. Mathematically, it is de-

fined as the inner product of signal $s(t)$ with $\Psi_{a,b}(t)$:

$$W_S(a,\ b) = \int_{-\infty}^{+\infty} s(t)\Psi^*_{a,b}(t)\mathrm{d}t, \tag{4}$$

where * denotes the complex conjugate. The signal $s(t)$ can be recovered from the wavelet coefficients $W_S(a, b)$ by an inverse wavelet transform given by[17]

$$s(t) = \frac{1}{C_\Psi}\int_{-\infty}^{+\infty}\int_{-\infty}^{+\infty} W_S(a,\ b)\Psi\left(\frac{t-b}{a}\right)\frac{\mathrm{d}a}{a^2}\,\mathrm{d}b, \tag{5}$$

provided that the constant C_Ψ is given by

$$C_\Psi = 2\pi\int_{-\infty}^{+\infty}\frac{|\hat{\Psi}(\omega)|^2}{\omega}\,\mathrm{d}w < +\infty, \tag{6}$$

where $\hat{\Psi}(\omega)$ denotes the Fourier transform of $\Psi(t)$.

For phase extraction from a real function (e.g., determination of instantaneous frequency), the most commonly used wavelet is the complex Morlet wavelet. It gives the smallest Heisenberg box[25] and has better resolution in scale and translation:

$$\Psi(t) = g(t)\exp(i\omega_0 t), \tag{7}$$

where $g(t) = \exp(-t^2/2)$. ω_0 is the mother frequency, the only parameter that has to be chosen. One consideration is that $\hat{\Psi}(0)$ is numerically negligible. This condition is verified when $\omega_0 > 5$. Here $\omega_0 = 2\pi$ is chosen to satisfy the admissibility condition [Eq. (6)] so that the wavelet function is able to remove the negative frequencies as well as avoid the dc contribution of the signals. In this study, CWT expands a one-dimensional intensity variation of certain pixels into a two-dimensional plane of scaling a (which is related to the temporal frequency) and position b (which is related to the time axis). Substituting Eqs. (2) and (7) into Eq. (4), one can express the wavelet transform of the intensity variation on pixel $P(x, y)$ as[26,27]

$$W_{xy}(a,\ b) = \frac{\sqrt{a}}{2}A_{xy}(b)(\hat{g}\{a[\zeta - \phi'_{xy}(b)]\} + \epsilon(b,\ \zeta)) \times \{\exp[i\phi_{xy}(b)]\}, \tag{8}$$

where $\zeta = \omega_0/a$, $\phi'_{xy}(b)$ is defined as the instantaneous frequency of the signal, and ϵ is a corrective term that is negligible if the following conditions are satisfied:

$$\frac{{\omega_0}^2}{|\phi'_{xy}(b)|^2}\frac{|A''_{xy}(b)|}{|A_{xy}(b)|} \ll 1, \tag{9}$$

$${\omega_0}^2\frac{|\phi''_{xy}(b)|}{|\phi'_{xy}(b)|^2} \ll 1. \tag{10}$$

The trajectory of maximum $|W_{xy}(a, b)|^2$ on the a–b plane is called a ridge. Because $|\hat{g}(\omega)|$ is maximum at $\omega = 0$ and if $A_{xy}(b)$ and $\phi'_{xy}(b)$ have small variations over the support of Ψ_{ab}, $\phi'_{xy}(b) \geq \Delta\omega/a$, and $\epsilon(b, \zeta)$ is negligible, $|W_{xy}(a, b)|^2$ reaches maximum when

$$\phi'_{xy}(b) = \zeta_{rb} = \frac{\omega_0}{a_{rb}}, \tag{11}$$

where a_{rb} denotes the value of a at instant b on the ridge. The wavelet transform on the ridge can then be expressed as

$$W_{xy}(a_{rb},\ b) \approx \frac{\sqrt{a_{rb}}}{2}A_{xy}(b)\hat{g}(0)\exp[i\phi_{xy}(b)]. \tag{12}$$

The phase value $\phi_{xy}(b)$ of wavelet transform $W_{xy}(a, b)$ on the ridge is relevant to the distance measured. For determining the phase variation $\Delta\phi$ between two rotating angles α_1 and α_2, an integration is processed on the instantaneous frequency $\phi'_{xy}(b)$, so that the phase-unwrapping procedure is avoided in both the temporal and the spatial domains. As only the phase variation is of interest, it is not necessary to consider the boundary condition of the integration. $H(x, y)$ in Eq. (2) then can be determined by

$$H(x,\ y) = \frac{p_0\Delta\phi}{2\pi(\cos\alpha_1 - \cos\alpha_2)}. \tag{13}$$

With a selected α_1, a series of $\Delta\phi$ can be obtained with different angles of α_2. $H(x, y)$ can be determined more accurately with least-squares fitting; subsequently, $h(x, y)$ is obtained by

$$h(x,\ y) = \frac{H(x,\ y)l}{d - H(x,\ y)}. \tag{14}$$

3. Experimental Illustration

Figure 2 shows the experimental setup. A specimen is placed on a movable platform, whose distance to the grating can be adjusted. A linear sinusoidal grating, positioned close to the specimen, is placed on a rotary indexing stage that has an accuracy of 0.0167°. A 150-W dc white-light source with an optical fiber illuminates the object at a certain angle. The moiré fringe patterns are recorded with a CCD camera whose optical axis is directed normal to the plane of the grating. Two specimens are measured in this study. One is an object with a stepped profile. A coin with small variation in the surface profile is used as another specimen to test the accuracy of the proposed method, and the result obtained is compared with that of the mechanical stylus method.

4. Results and Discussion

Figure 3(a) shows the dimensions of the object with a stepped profile. The heights of two steps are 1.62 $\pm$ 0.01 and 3.31 $\pm$ 0.01 mm when measured from the

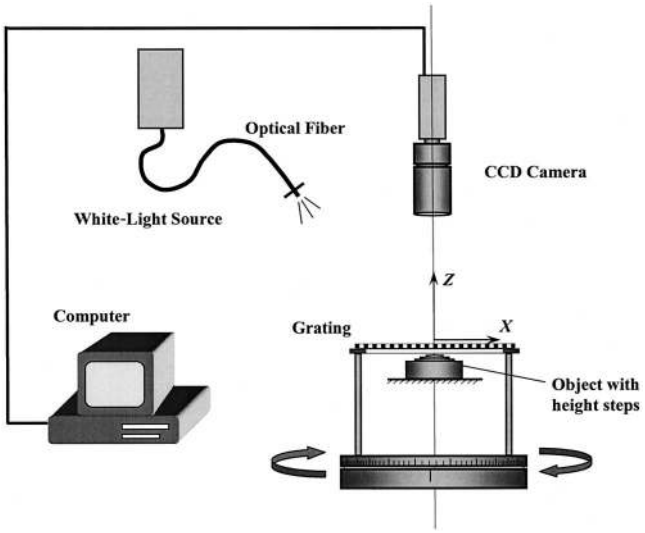

Fig. 2. Experimental setup.

topmost surface with a dial gauge. Figure 3(b) shows the initial test object without a grating in front. Owing to the shading problem that is inherent to all triangulation techniques, only an area without shading is selected for processing. The frequency of the grating is 4 lines/mm. The distance d and l (shown in Fig. 1) are 175 and 355 mm, respectively. The fringe patterns are captured at a right angle by a CCD

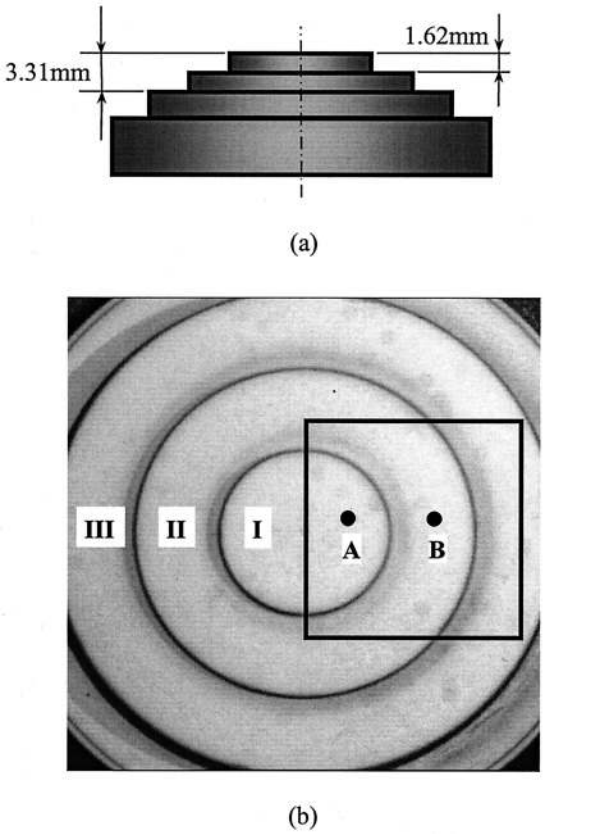

Fig. 3. (a) Dimension of the height step. (b) Area of interest on a specimen with a height step.

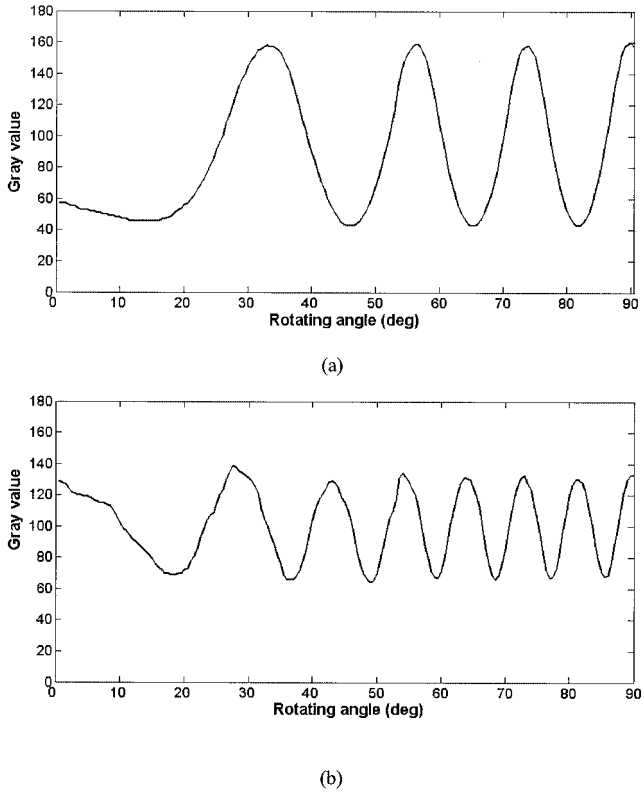

Fig. 4. (a) Gray-value variation of point A; (b) gray-value variation of point B.

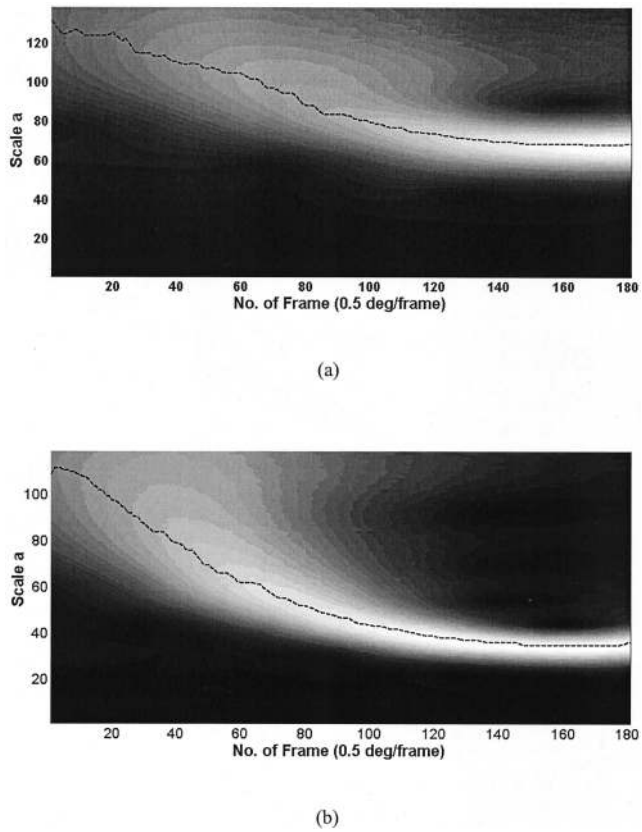

Fig. 5. (a) Modulus of the Morlet wavelet transform at point A; (b) modulus of the Morlet wavelet transform at point B.

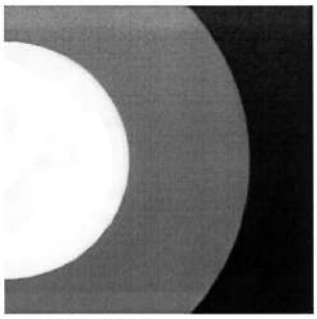

(a)

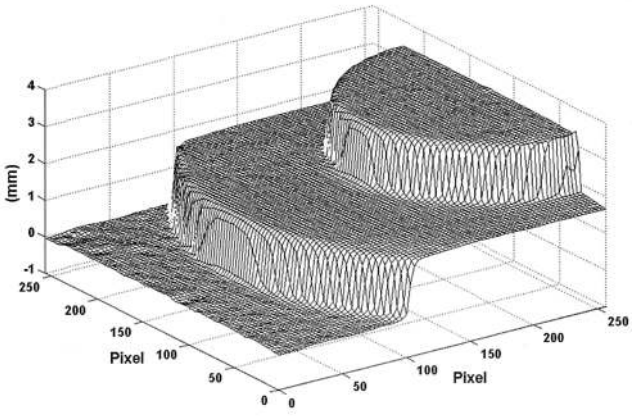

(b)

Fig. 6. (a) Gray-scale map of the area of interest; (b) 3-D plot of the area of interest.

(a)

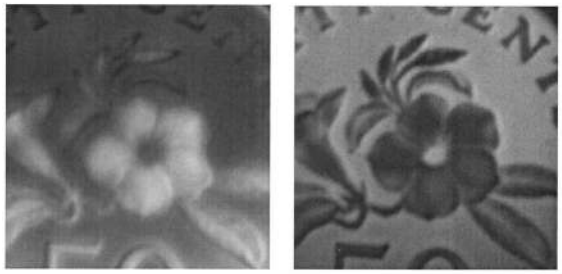

(b) (c)

Fig. 7. (a) Area of interest on a coin; typical moiré fringe patterns at (b) $\alpha = 30°$ and (c) $\alpha = 40°$.

camera when the grating is rotated from $\alpha = 0°$ at increments of $\Delta\alpha = 0.5°$. We captured 180 images for processing. A 5×5 mean mask is applied to remove the high-frequency grating lines on the images. At each pixel, 180 sampling points along the time axis are obtained. Figures 4(a) and 4(b) show the gray-value variation of points A and B [see Fig. 3(b)], respectively. A lower frequency of gray-value variation is observed at point A than at point B, which implies $h(x, y)$ at point A is smaller than that at point B. Owing to the diffraction effect, the fringe contrast is low when the distance between the object and the grating is large. Figure 4(a) shows that point A has much better contrast than point B. However, only temporal frequencies are considered as they contain information of the instantaneous frequencies, from which the phase variation $\Delta\phi$ can be derived. The moduli of the Morlet wavelet transform of the intensity variation of points A and B are shown in Figs. 5(a) and 5(b), respectively. The dashed curve shows the ridge of the wavelet transformation where the maximum modulus is found. In this study, α_1 in Eq. (13) is selected as 30°. α_2 varies from 30.5° to 70°. $H(x, y)$ on each point is obtained by a least-squares fitting; subsequently, the heights $h(x, y)$ at steps I, II, and III [see Fig. 3(b)] are obtained as 1.97 ± 0.01, 3.59 ± 0.02, and 5.27 ± 0.03 mm, respectively. Figure 6(a) shows the gray-scale map representing the height difference. The height steps shown in Fig. 3(a) are 1.62 ± 0.03 and 3.30 ± 0.04 mm. The average discrepancy is 0.3% when results are compared with those from the dial gauge measurement. Figure 6(b) shows a 3D reconstruction of the area of interest on the object. A relatively high unevenness is observed at step III; this is due to the lower contrast of the intensity variation, and the noise effect is more obvious in this case.

The proposed wavelet analysis method is also applied to a coin of 24.5-mm diameter [shown in Fig. 7(a)] to test the resolution of the proposed method. A small area of interest containing 300×300 pixels [also indicated in Fig. 7(a)] is cropped. A grating with a pitch of 6 lines/mm is selected. The distance d and l (shown in Fig. 1) are, respectively, 310 and 160 mm. The fringe patterns are also captured at a right angle by a CCD camera when the grating is rotated at increments of $\Delta\alpha = 0.5°$. Similarly, 180 images are captured for processing. A 3×3 mean mask is also applied to remove the high-frequency grating lines on the images. At each pixel, 180 sampling points along the time axis are obtained. The processes are similar to those used with the object mentioned above. Figures 7(b) and 7(c) show the typical moiré fringe patterns at $\alpha = 30°$ and $\alpha = 40°$, respectively. The gray-scale map representing the contour of the coin is

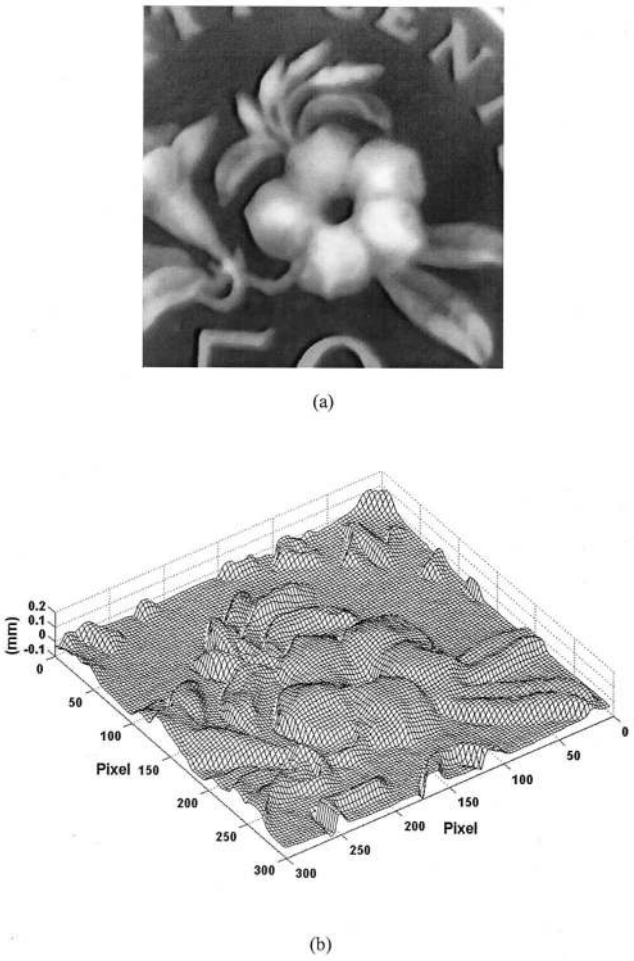

Fig. 8. (a) Gray-scale map of the area of interest on a coin; (b) 3-D plot of the area of interest.

given in Fig. 8(a). Figure 8(b) is the 3D plot of the area of interest. To verify the accuracy of the contour measurement by the proposed method, we carry out a comparison between the proposed temporal wavelet method and the mechanical stylus method. Figure 9 shows a comparison of the profile on cross section C–C [see Fig. 7(a)]. The results of the contour measurement compared well with the mechanical stylus method, and the accuracy of the proposed method is

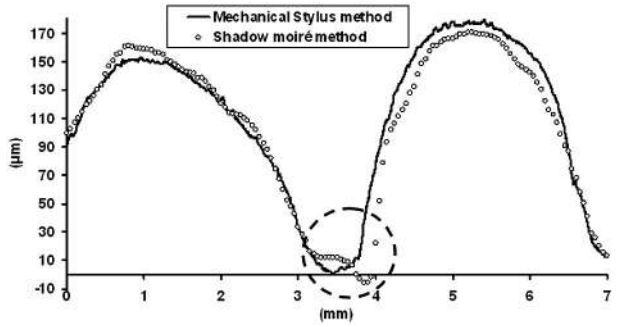

Fig. 9. Comparison of the surface profile of a coin at cross section C–C between the shadow moiré and the mechanical stylus methods.

of the order of 10 μm. However, a slightly large error (shown by circles in Fig. 9) is observed at the shadow part of the profile.

It is worth noting that only sampling points between 30° and 70° are used in the calculation. It is not necessary to capture the fringe patterns in the range of 0° to 90° as shown above. However, the CWT will generate a large error at the boundary. To remove the border effect, we extend the intensity variation signal on each pixel at its left- and right-hand edges. A linear predictive extrapolation method[28] is selected in this study. The advantage of this extrapolation method is that the phase and frequency of intensity variations are maintained. After the CWT has been carried out on the extended data, the wavelet coefficients are truncated appropriately, and accurate results can still be obtained.

The CWT maps a one-dimensional intensity variation signal to a two-dimensional plane of time and frequency and extracts the frequencies with the highest energy at different instants. As the frequency variation of the grating during rotation is nonlinear, the CWT is more suitable to obtain the instantaneous frequency of the intensity change. A consistent angle step, which is much easier to achieve, can be adopted for automatic measurement. However, the CWT has its own drawback. Although some fast-converging iterative algorithms[29] are introduced by some researchers and it is not necessary to explore the whole time–frequency plane, CWT is a time-consuming process, and high computing speed and memory are required. The computation time is approximately ten times larger than that of the temporal Fourier transform. This is the main limitation of applying the temporal wavelet technique to industrial inspection in which speed is always a concern. However, this disadvantage becomes insignificant owing to the rapid improvement in the capacity of computers.

5. Concluding Remarks

In this paper a novel method based on temporal wavelet analysis is presented to retrieve the profile of objects with discontinuous height steps. A series of images is captured when a grating is rotated above the specimen. As the distance between the specimen and the grating is retrieved pixel by pixel with the continuous Morlet wavelet transform, both temporal and spatial phase unwrapping is avoided. Furthermore, compared with Fourier analysis, the CWT has its own advantages when nonlinearity of intensity variation is observed during rotation of the grating. High-quality surface profiles are retrieved. The averaged discrepancy is less than 0.5%. The same algorithm is also applied to a coin with an unevenness of 0.2 mm, and the maximum discrepancy is around 5%. The resolution of the surface profile from the proposed method is comparable with that from shadow moiré by phase shifting. The proposed method could also be applied to wavelength-scanning interferometry or measurement of continuous deformation.

References

1. D. M. Meadows, W. O. Johnson, and J. B. Allen, "Generation of surface contours by moiré patterns," Appl. Opt. **9,** 942–947 (1970).
2. H. Takasaki, "Moiré topography," Appl. Opt. **9,** 1467–1472 (1970).
3. G. Mauvoisin, F. Bremand, and A. Lagarde, "Three-dimensional shape reconstruction by phase-shifting shadow moiré," Appl. Opt. **33,** 2163–2169 (1994).
4. X. Xie, M. J. Lalor, D. R. Burton, and M. M. Shaw, "Four-map absolute distance contouring," Opt. Eng. **36,** 2517–1520 (1997).
5. T. Yoshizawa and T. Tomisawa, "Shadow moiré topography by means of the phase-shift method," Opt. Eng. **32,** 1668–1674 (1993).
6. L. Jin, Y. Kodera, T. Yoshizawa, and Y. Otani, "Shadow moiré profilometry using the phase-shifting method," Opt. Eng. **39,** 2119–2123 (2000).
7. J. Degrieck, W. Van Paepegem, and P. Boone, "Application of digital phase-shift shadow moiré to micro deformation measurements of curved surface," Opt. Lasers Eng. **36,** 29–40 (2001).
8. R. Henan, A. Tagliaferri, and R. Torroba, "A contouring approach using single grating digital shadow moiré with a phase stepping technique," Optik (Stuttgart) **110,** 199–201 (1999).
9. J. M. Huntley, "Challenges in phase unwrapping," in *Trends in Optical Nondestructive Testing and Inspection*, P. K. Rastogi and D. Inaudi, eds. (Elsevier Science, Amsterdam, 2000), pp. 37–44.
10. L. H. Jin, Y. Otani, and T. Yoshizawa, "Shadow moiré profilometry by frequency sweeping," Opt. Eng. **40,** 1383–1386 (2001).
11. Y. Y. Hung, C. Y. Liang, A. J. Durelli, and J. D. Hovanesian, "A shadow-moiré method with continuously variable sensitivity," Mech. Res. Comm. **4,** 157–162 (1977).
12. Y. Y. Hung and H. M. Shang, "A novel shadow moiré technique for absolute surface shape measurement," in *Proceedings of the SEM Ninth International Conference on Experimental Mechanics* (Society for Experimental Mechanics, Orlando, Fla., 2000), pp. 96–99.
13. H. Tiziani, B. Franze, and P. Haible, "Wavelength-shift speckle interferometry for absolute profilometry using a mode-hop free external cavity diode laser," J. Mod. Opt. **44,** 1485–1496 (1997).
14. M. Takeda and H. Yamamoto, "Fourier-transform speckle profilometry: three-dimensional shape measurements of diffuse objects with large height steps and/or spatially isolated surfaces," Appl. Opt. **33,** 7829–7837 (1994).
15. C. Quan, Y. Fu, and C. J. Tay, "Determination of surface contour by temporal analysis of shadow moiré fringes," Opt. Commun. **230,** 23–33 (2004).
16. M. Takeda, H. Ina, and S. Kobayashi, "Fourier-transform method of fringe-pattern analysis for computer-based topography and interferometry," J. Opt. Soc. Am. **72,** 156–160 (1982).
17. I. Daubechies, *Ten Lectures on Wavelets* (Society for Industrial and Applied Mathematics, Philadelphia, Pa., 1992).
18. A. Federico and G. H. Kaufmann, "Evaluation of the continuous wavelet transform method for the phase measurement of electronic speckle pattern interferometry fringes," Opt. Eng. **41,** 3209–3216 (2002).
19. Y. Morimoto, M. Fujigaki, and S. Yoneyama, "Shape, stress, and strain measurement using phase analysis of grating or fringe patterns," in *Third International Conference on Experimental Mechanics*, X. Wu, Y. Qin, J. Fang, and J. Ke, eds., Proc. SPIE **4537,** 47–52 (2002).
20. K. Qian, H. S. Seah, and A. Asundi, "Instantaneous frequency and its application to strain extraction in moiré interferometry," Appl. Opt. **42,** 6504–6513 (2003).
21. L. R. Watkins, S. M. Tan, and T. H. Barnes, "Determination of interferometer phase distributions by use of wavelets," Opt. Lett. **24,** 905–907 (1999).
22. X. Colonna de Lega, "Continuous deformation measurement using dynamic phase-shifting and wavelet transform," in *Applied Optics and Optoelectronics 1996*, K. T. V. Grattan, ed. (Institute of Physics, Bristol, UK, 1996), pp. 261–267.
23. M. Cherbuliez, P. Jacquot, and X. Colonna de Lega, "Wavelet processing of interferometric signal and fringe patterns," in *Wavelet Applications in Signal and Image Processing VII*, M. A. Unser, A. Aldroubi, and A. F. Laine, eds., Proc. SPIE **3813,** 692–702 (1999).
24. X. Colonna de Lega, "Processing of non-stationary interference patterns: adapted phase shifting algorithms and wavelet analysis. Application to dynamic deformation measurements by holographic and speckle interferometry," Theses no. 1666 (Swiss Federal Institute of Technology, Lausanne, Switzerland, 1997).
25. S. Mallat, *A Wavelet Tour of Signal Processing* (Academic, San Diego, Calif., 1998).
26. C. J. Tay, C. Quan, Y. Fu, and Y. Huang, "Instantaneous velocity displacement and contour measurement by use of shadow moiré and temporal wavelet analysis," Appl. Opt. **43,** 4164–4171 (2004).
27. Y. Fu, C. J. Tay, C. Quan, and L. J. Chen, "Temporal wavelet analysis for deformation and velocity measurement in speckle interferometry," Opt. Eng. **43,** 2780–2787 (2004).
28. W. H. Press, S. A. Teukolsky, W. T. Vetterling, and B. P. Flannery, *Numerical Recipes in FOTRAN*, 2nd ed. (Cambridge U. Press, Cambridge, UK, 1992), Chap. 13.
29. M. Cherbuliez and P. Jacquot, "Phase computation through wavelet analysis: yesterday and nowadays," in *Fringe 2001*, W. Osten and W. Juptner, eds. (Elsevier, Paris, 2001), pp. 154–162.